Supplemental Data

Conventional kernel method

For the conventional kernel method, the voxel intensity value extracted from the mean image z_a (Eq. 7) was used for generating the kernel matrix using 50 nearest neighbors within a $9 \times 9 \times 9$ local region. The radial Gaussian kernel function was used.

4D DIP method

The DIP model was built based on a modified 3D U-Net architecture (*26*). The mean image z_a was used as the input of the model, and each frame z_m was the training label. We used the Adam optimizer with 0.001 learning rate and 10,000 training epochs because of the better performance in our experiments.

ROI locations of bone marrow and muscle

Spine bone marrow: an average of ten spine sections across thoracic, lumbar, and sacrum vertebrae

Pelvic bone marrow: an average of four ROIs, two on the left and two on the right

Muscle: an average of two ROIs of left and right thighs

SUPPLEMENTAL TABLE 1

Basic information on individual subjects

Subject	Age (year)	Sex	BMI (kg/m^2)	Scan protocol
GUC01	64	M	32	0-60 minutes
GUC02	61	M	26.3	0-60 minutes
GUC03	64	M	25.3	0-60 minutes
GUC04	76	M	20.1	0-60 minutes
GUC05	70	M	24.3	0-60 minutes
GUC06	73	M	25.6	0-60 minutes
GUC07	56	M	25.7	0-60 minutes
GUC08	75	M	21	0-60 minutes
GUC09	82	F	35.5	0-60 minutes
GUC10	65	F	18.3	0-60 minutes
HS01	78	M	24.4	0-60 minutes
HS02	62	M	29.5	0-60 minutes
HS03	63	M	24	0-60 minutes
HS04	73	M	23.8	0-60 minutes
HS05	60	F	26.4	0-60 minutes
HS06	67	F	25.5	0-60 minutes
HS07	67	M	23.3	0-60 minutes
HS08	61	F	20.2	0-60 minutes
HS09	60	F	33.7	0-60 minutes
HS10	61	F	23.1	0-60 minutes
HS11	64	M	25.2	0-60 minutes
HS12	58	M	37.6	0-60 minutes
Other01	42	M	35.4	60-80 minutes
Other02	71	M	20.5	120-140 minutes

GUC: genitourinary cancer HS: Healthy subject
Other01: lymphoma patient, Other02: Lung cancer patient

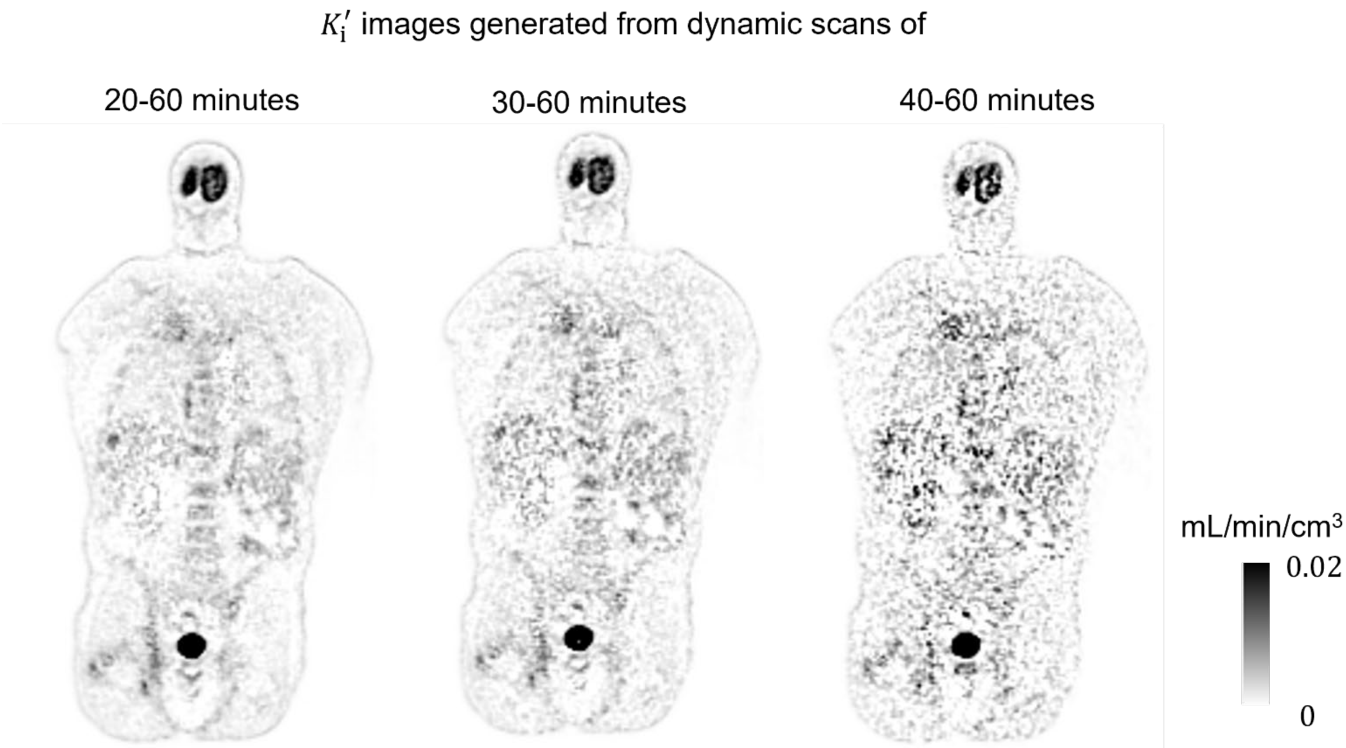

SUPPLEMENTAL FIGURE 1. RP K_i' images generated from dynamic scans of 20-60 minutes, 30-60 minutes, and 40-60 minutes without using post-reconstruction noise-reduction methods. The noise level is higher when the scan duration is reduced.

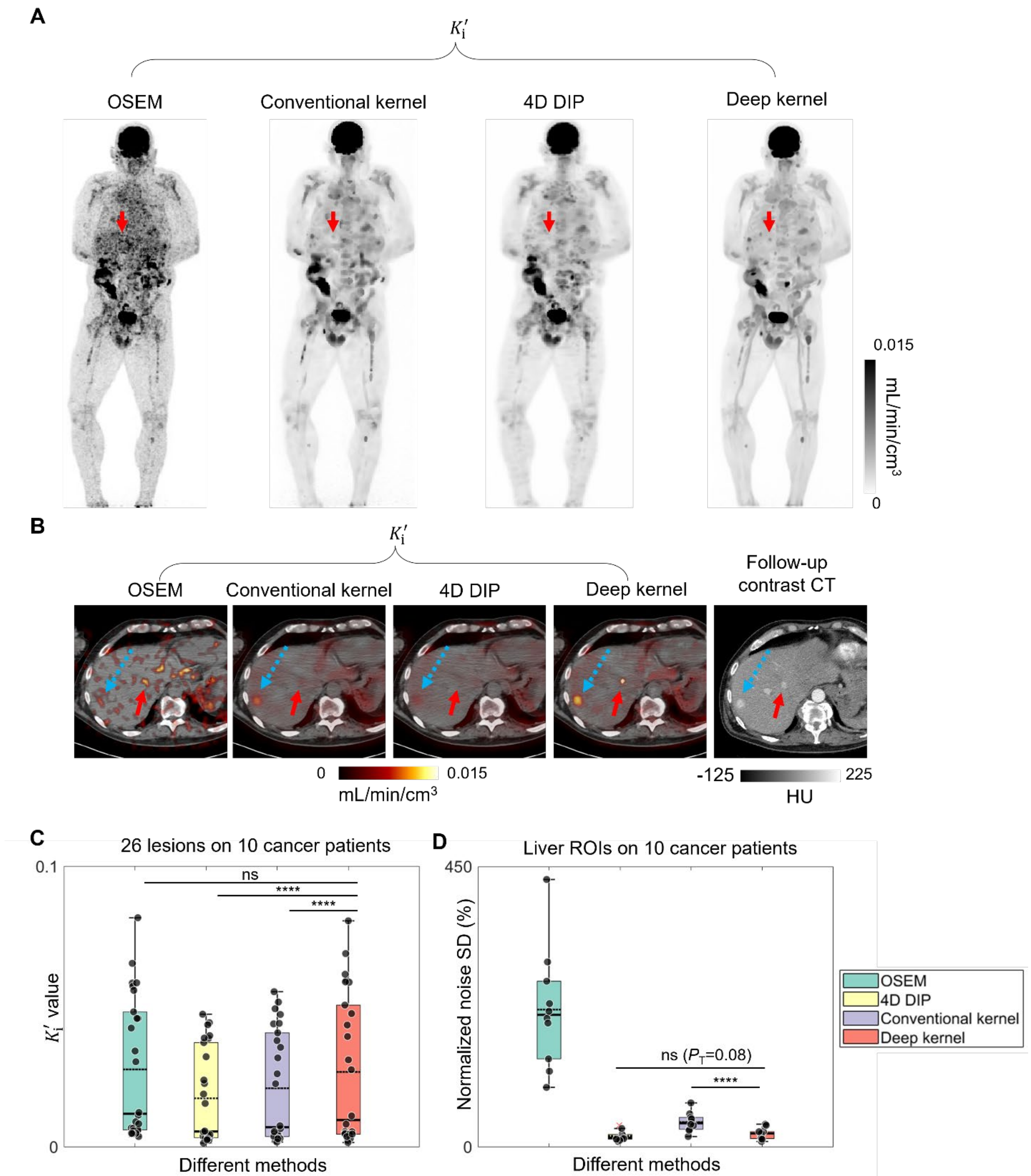

SUPPLEMENTAL FIGURE 2. Comparison of different methods for generating an RP K_i' image (GUC03). (A) Maximum intensity projection of K_i' parametric images generated using four methods. A liver lesion is pointed by the red arrow. (B) Comparison for a transverse fused slice showing liver lesions which were confirmed on a follow-up contrast CT. The K_i' images were superimposed on CT component of the PET/CT. Group comparisons of (C) lesion K_i' values (number: 26) and (D) normalized background (liver) noise SD on 10 cancer patients by using paired t-test. ****: *P*<0.0001, ns: *P*>0.05.

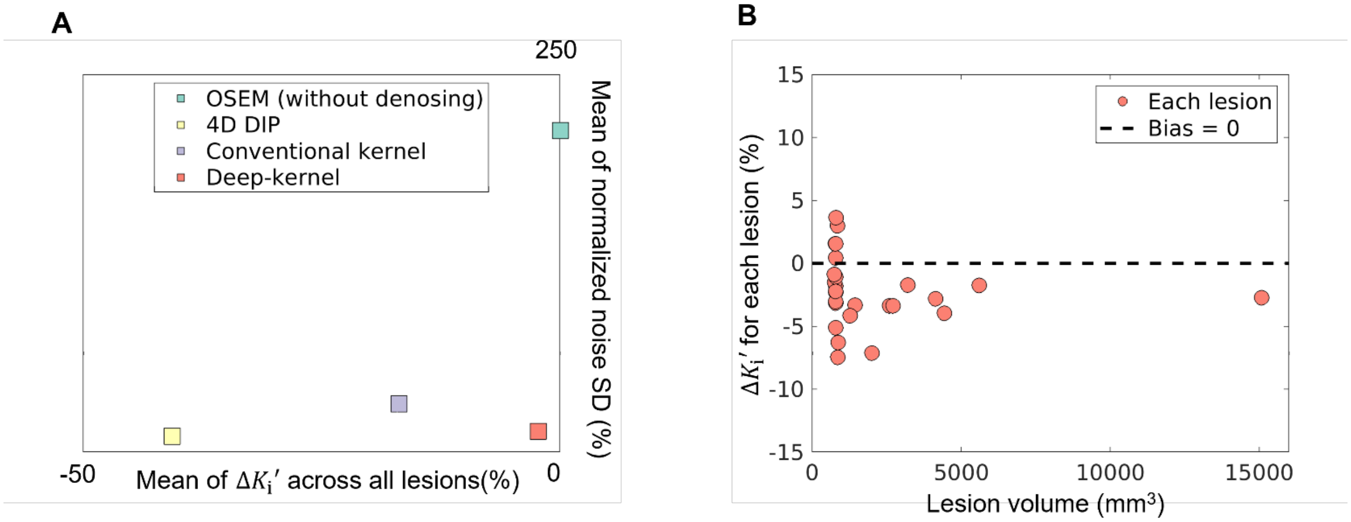

SUPPLEMENTAL FIGURE 3. Impact of the three denoising methods for RP K_i' quantification. The OSEM method (without denoising) was considered the reference to calculate the bias. (A) The scatter plot between the averaged bias in lesion K_i' and the liver background noise SD by using different methods; (B) The scatter plot between the $\Delta K_i'$ of each lesion and lesion volume with deep-kernel method. All 26 lesions from 10 cancer patients (consistent with Supplemental Fig. 2) were used and the lesion volume ranged from 740 mm^3 to 15077 mm^3.

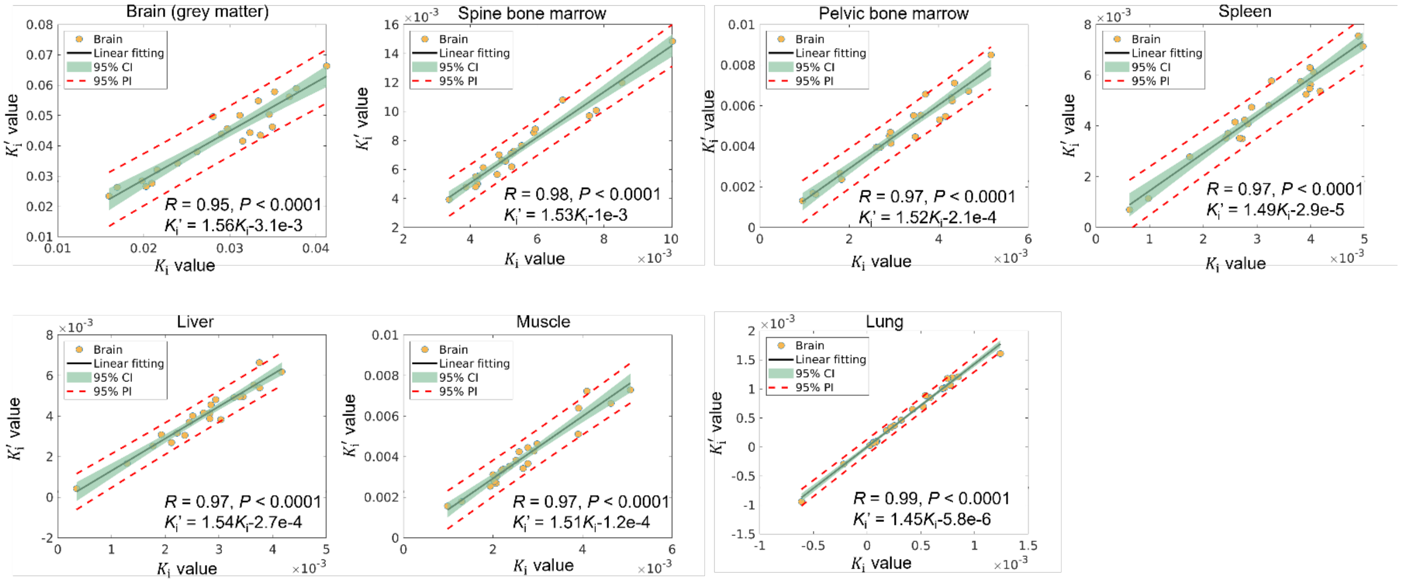

SUPPLEMENTAL FIGURE 4. The correlation plot for each organ ROI across 22 subjects. The fitting slope, intercept, CI, PI, *R*, and *P*-value were included.

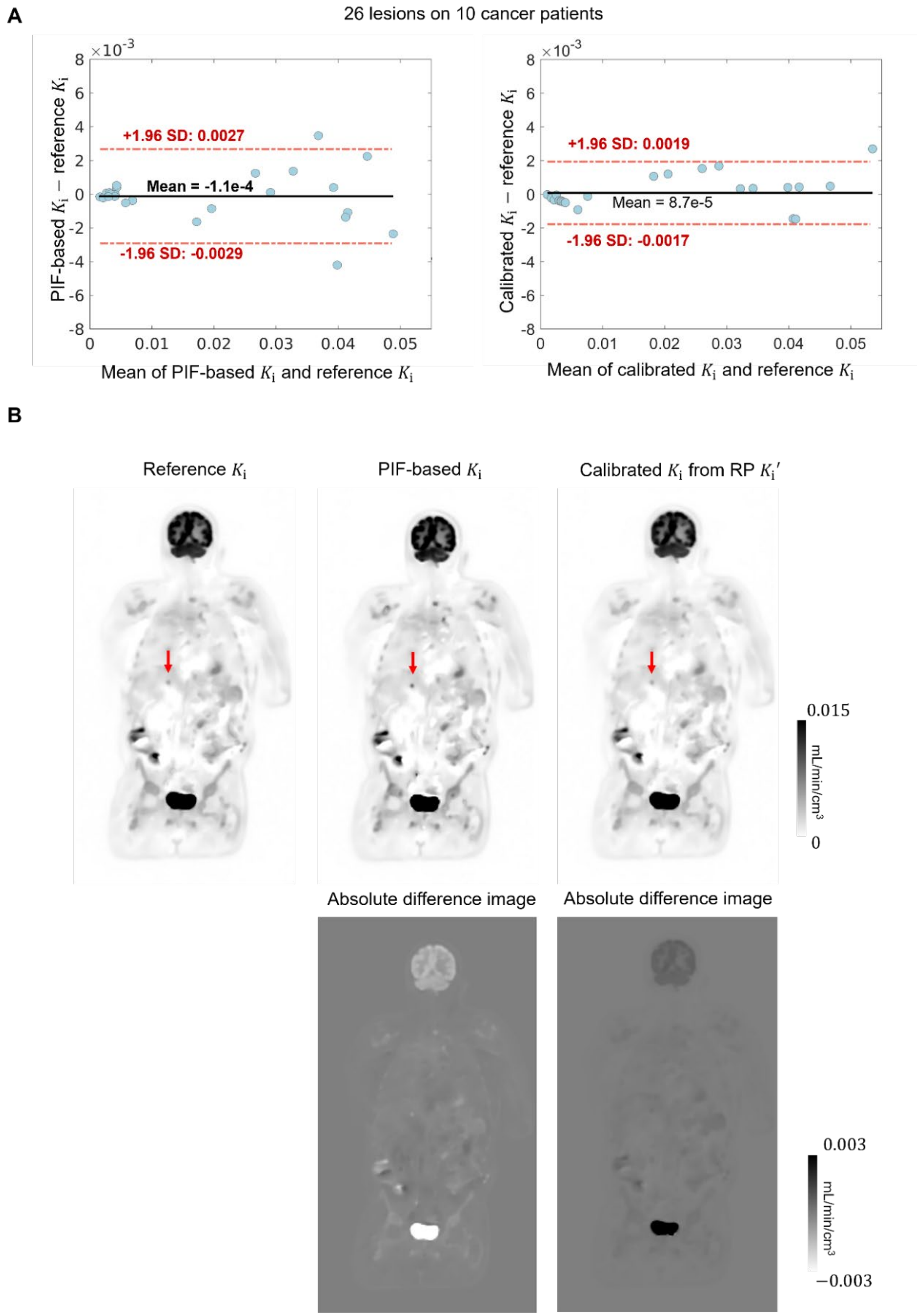

SUPPLEMENTAL FIGURE 5. Quantitative comparison between the PIF-based K_i and the calibrated K_i from RP K_i', with the standard Patlak K_i being the reference. (A) The Bland–Altman plots of lesion ROI quantification for 10 cancer patients (left:) between reference K_i and PIF-based K_i, and (right:) between reference K_i and calibrated K_i; (B) Comparison of the parametric image of reference K_i, PIF-based K_i, and calibrated K_i for a cancer patient. Their absolute difference images were included (GUC03).